# Chalcogenide-based van der Waals epitaxy: Interface conductivity of tellurium on Si(111)

Felix Lüpke,[1,2] Sven Just,[1,2] Gustav Bihlmayer,[1,2,3] Martin Lanius,[1,2] Martina Luysberg,[1,2] Jiří Doležal,[4] Elmar Neumann,[1,2] Vasily Cherepanov,[1,2] Ivan Ošt'ádal,[4] Gregor Mussler,[1,2] Detlev Grützmacher,[1,2] and Bert Voigtländer[1,2,*]

[1]*JARA–FIT, 52425 Jülich, Germany*

[2]*Peter Grünberg Institut, Forschungszentrum Jülich, 52425 Jülich, Germany*

[3]*Institute for Advanced Simulation, Forschungszentrum Jülich, 52425 Jülich, Germany*

[4]*Department of Surface and Plasma Science, Faculty of Mathematics and Physics, Charles University, 182 00 Prague 8, Czech Republic*

(Received 20 January 2017; published 5 July 2017)

We present a combined experimental and theoretical analysis of a Te rich interface layer which represents a template for chalcogenide-based van der Waals epitaxy on Si(111). On a clean Si(111)-(1 × 1) surface, we find Te to form a Te/Si(111)-(1 × 1) reconstruction to saturate the substrate bonds. A problem arising is that such an interface layer can potentially be highly conductive, undermining the applicability of the on-top grown films in electric devices. We perform here a detailed structural analysis of the pristine Te termination and present direct measurements of its electrical conductivity by *in situ* distance-dependent four-probe measurements. The experimental results are analyzed with respect to density functional theory calculations and the implications of the interface termination with respect to the electrical conductivity of chalcogenide-based topological insulator thin films are discussed. In detail, we find a Te/Si(111)-(1 × 1) interface conductivity of $\sigma_{2D}^{Te} = 2.6(5) \times 10^{-7}$ S/□, which is small compared to the typical conductivity of topological surface states.

DOI: 10.1103/PhysRevB.96.035301

In recent years, chalcogenide van der Waals (vdW) thin films have emerged as potential disruptive technologies in several fields of applications [1–3]. Among them are topological insulators (TIs) where the spin-momentum locking of topological surface states (TSS) prohibits direct backscattering and makes them an ideal candidate for low-power spintronics and quantum computing [1,4]. The most promising materials for such applications at room temperature are $Bi_2Se_3$, $Bi_2Te_3$, and $Sb_2Te_3$ due to their pronounced band gap [1,5]. For the successful utilization of the auspicious TSS properties in electronic devices it is necessary that an electrical current is transmitted predominantly by these surface states. Hereby, the TI bulk conductivity can play a significant role by the formation of a parasitic parallel conduction channel practically bypassing the TSS, as extensively studied in recent years [6,7]. In consequence, the growth of $Bi_2Se_3$, $Bi_2Te_3$, and $Sb_2Te_3$ TI thin films by molecular-beam epitaxy has become a crucial tool, which allows precise TI bulk and surface engineering and a high surface-to-bulk ratio [8,9]. A common substrate for such growth of TI films is Si(111), where an initial saturation of the substrate bonds is required to form a template for the vdW epitaxy [8,10,11]. The TI film is then grown on top of this template layer and is only weakly bound by vdW interaction to the underlying structure with a sharp interface between the TI film and the substrate [11]. The problem arising is that such terminations of Si can have a high conductivity resulting in an additional parasitic conductivity of the interface layer between the TI film and the substrate [12–16]. Furthermore, such an interface transport channel is difficult to distinguish from contributions of the TSS channel at the bottom of the TI film by conventional transport measurements.

We present here a detailed experimental and theoretical analysis of the structure and charge transport properties at the Te interface of a $Bi_2Te_3$-based thin film grown on a Si(111) substrate. We first investigate the sample cross section in scanning transmission electron microscopy (STEM) and subsequently prepare the interface termination of the substrate without the TI thin film on top. Here, the combination of low-energy electron diffraction (LEED) and multitip scanning tunneling microscopy (STM) allows us to directly quantify the structural and charge transport properties of the pristine, atomically thin Te layer *in situ*. The results are interpreted with respect to density functional theory (DFT) calculation which we performed in the context of the experimentally observed structures.

To analyze the atomic structure of the Te interface layer, we use a cross-sectional aberration corrected STEM (FEI Titan 80-200) for which sample cross sections are prepared by focused ion-beam (FIB) etching using 5 keV Ga ions and subsequent Ar ion milling (Fishione NanoMill) to reduce the FIB-induced damage. High-resolution STEM images are made in high-angle annular dark field mode where the contrast scales approximately quadratic with the atomic number $Z$. Figure 1(a) shows a STEM measurement of the TI thin film grown on Si(111) [8]. In detail, the film shown here is $Bi_1Te_1$ which is grown by an initial saturation of the Si(111) substrate with Te as described below, followed by the codeposition of Bi and Te [17]. The result is in an alternating stacking of $Bi_2Te_3$ quintuple layers and Bi(111) bilayers as indicated in Fig. 1(b). The substrate interface hereby is identical to that of a pure $Bi_2Te_3$ film and is reported to be Te rich [8,11]. From the STEM measurements, we find that the Te interface layer atoms, which are deposited prior to the TI film growth to saturate the Si(111) surface, are located directly above the underlying Si(111) substrate atoms, which can be explained by adsorption of Te at the T1 (on top) site corresponding to a (1 × 1) structure. The first layer of the TI film on top of the Te interface is decoupled from the interface layer as evident by its relaxed crystal structure corresponding to the TI bulk lattice parameters [8]. A line scan perpendicular to the interface

*Corresponding author: b.voigtlaender@fz-juelich.de

 

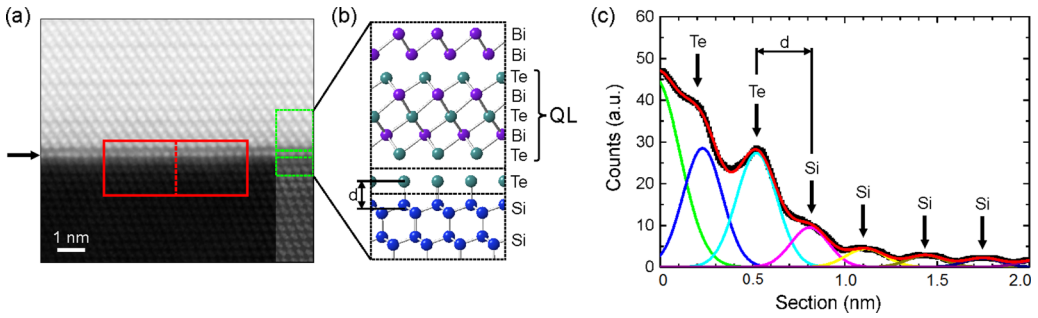


FIG. 1. (a) STEM image of the $Bi_1Te_1$/Si(111) interface with the atom row of the Te interface indicated by an arrow. The viewing direction with respect to the Si substrate is $(1\bar{1}0)$ and Bi atoms appear brightest due to $\sim Z^2$ contrast. Near the right edge of the image the overall brightness in the region of the substrate was increased to accentuate the Si atom rows. (b) Schematic of the atomic layers near the interface in (a). A quintuple layer (QL) corresponding to $Bi_2Te_3$ and the Si-Te interlayer distance $d$ are indicated. (c) Line scan perpendicular to the interface averaged over the red frame indicated in (a) (black dots) and corresponding multiple Gaussian peak fit (red curve). The Gaussian peak fits of the Te interface layer and first Si bilayer result in a Si-Te spacing of $d = 2.88(3)$ Å.

layer is shown in Fig. 1(c). The peak positions corresponding to the atomic layers are analyzed by fitting multiple Gaussian peaks. Hereby, Si peaks correspond to the center of mass of the Si(111) bilayers. We measure the distance between the center of mass of the topmost Si(111) bilayer and the Te interface layer to be $d = 2.88(3)$ Å.

Due to the weak vdW coupling of the TI film to the substrate, the properties of the interface layer are expected to be unaffected by the growth of the TI film on top. In the next step, we therefore prepare the sole Te termination of the Si(111) substrate, to further investigate the structural and transport properties of the Te interface. Hereby, we use the same preparation procedure as for the sample mentioned above, on which also the TI film was grown: A low doped $p$-Si(111) substrate with $\rho_{\text{bulk}} = 22\,\text{k}\Omega\,\text{cm}$ was cleaned using a RCA type procedure [8]. After the final hydrofluoric acid (HF) dip the sample was immediately introduced into the STM/LEED analysis chamber ($p \approx 1 \times 10^{-10}$ mbar). The hydrogen was then desorbed at 700 °C for 10 min. During this step, LEED monitoring shows a clear Si(111)-$(1 \times 1)$ surface structure corresponding to the unreconstructed Si(111) substrate. The reactive Si(111)-$(1 \times 1)$ surface is then passivated by Te at a sample temperature of 270 °C and a Te rate of 1 ML/min for 10 min [18]. Here, the number of atoms in 1 ML corresponds to the number of atoms on the Si(111)-$(1 \times 1)$ surface ($7.84 \times 10^{14}$ atoms/cm$^2$, i.e., half a bilayer). The Te deposition is stopped by closing the evaporator and quenching the sample to room temperature. After the Te deposition, LEED still shows a $(1 \times 1)$ pattern as shown in Fig. 2(a) and in agreement with the STEM measurements. The intensity of the LEED pattern is comparable to that of the pure Si(111)-$(1 \times 1)$ surface before Te deposition, indicating a crystalline quality of the Te layer. Note that in the LEED images a diffuse background intensity is observed, both before and after deposition of the Te, which we attribute to a high surface roughness resulting from the HF etching [19,20]. We conclude that we have prepared a single atomic layer of Te on the sample surface resulting in a Te/Si(111)-$(1 \times 1)$ reconstruction: Due to the high reactivity of the unreconstructed Si(111) surface, it is certain that at least one layer of Te sticks to the sample surface, in agreement with literature [30]. Furthermore, we confirmed in a separate experiment, where we first deposited ~20 ML of Te at room temperature and then heated the sample to 270 °C under LEED investigation, that no Te beyond the first layer sticks to the sample surface at this temperature. In detail, in this experiment the initial diffuse LEED image begins to show spots at a sample temperature above ~200 °C, identical to the LEED image for deposition of 1 ML of Te at elevated temperature.

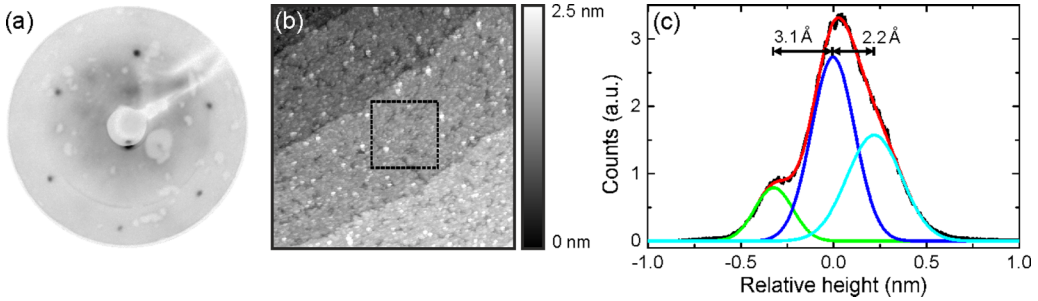


FIG. 2. (a) LEED image of the Te/Si(111) surface recorded at an electron energy of 30 eV. We observe spots corresponding to a $(1 \times 1)$ structure with respect to the Si(111) surface. (b) Topography of the Te/Si(111)-$(1 \times 1)$ surface showing Si substrate steps with a height of 3.1 Å. The single terraces are found to be rough due to holes in the surface and clusters of additional material on top (sample bias +2 V, 70 pA, scan size 800 nm). (c) Height distribution in the square indicated in (b) with a multiple Gaussian peak fit. The differences between the peak positions are 3.1 and 2.2 Å, corresponding to the average depth of the holes and height of the excess material on top, respectively.

Subsequent STM scans of the sample surface show substrate steps of 3.1 Å height, corresponding to monoatomic steps of the Si(111) surface [Fig. 2(b)]. Hereby, a monoatomic step corresponds to the distance between neighboring bilayers of the Si(111) surface. The terrace width of ∼300 nm between steps is in accordance with the miscut of the Si(111) wafer. On the terraces, we observe pits and adsorbates, where we expected the additional material on top of the film to be additional Te adatoms and remainings of the HF cleaning procedure [19]. The average height of the adsorbates we find to be 2.2 Å as shown in Fig. 2(c). From the same graph, we also find that the pits are 3.1 Å in depth corresponding to the monoatomic step height of the Si(111) surface. Such pits and adsorbates, associated with a general surface roughening, are reported to result from the HF cleaning procedure [20,21]. Although we are not able to atomically resolve the Te/Si(111)-(1 × 1) structure in STM, we assume that the Te termination is intact also inside of the pits because the Te deposition should be uniform throughout the surface. The observed surface roughness and adsorbates are also in agreement with the diffuse background intensity in the LEED measurements.

In order to further evaluate the experimental observations, we performed DFT calculations in the local density approximation [22]. We employed the full potential linearized augmented plane-wave method in thin-film geometry [23] as implemented in the FLEUR code [24]. By deposition of a variable amount of Te atoms on the Si(111) surface (modeled by a ten layer film), we calculated two stable surface configurations corresponding to a $p(1 \times 1)$ and $c(2 \times 2)$ reconstruction, respectively. We find the predicted Te/Si(111)-(1 × 1) configuration to be in excellent agreement with our experimental results, while the structure of the $c(2 \times 2)$ reconstruction contradicts our experimental observations. In principle, a $c(2 \times 2)$ Te coverage would be ideal to saturate all dangling bonds and results in an insulating interface. However, the Si-Te interlayer distance of 1.9 Å is in variance with the experimental findings. We have also checked the possibility that this $c(2 \times 2)$ ordered layer is "hidden" in the experiment (e.g., due to the formation of rotational domains) and covered by an extra Te layer. This configuration, however, would place the extra Te layer 4.0 Å above the Si substrate, being also incompatible with the experiment. Finally, we checked different positions of $p(1 \times 1)$ ordered Te layers and found that the hollow (T4) position is almost 1 eV higher in energy than the on-top (T1) position and gives a much too small Si-Te interlayer distance of 1.9 Å. It is therefore also ruled out to be present in our experiments. In consequence, the calculations of the Te/Si(111)-(1 × 1) surface result in the adsorption position of the Te atoms at the on-top (T1) site, corresponding to the STEM and LEED results. In this configuration, the distance between the center of mass of the topmost Si(111) bilayer and the Te interface layer in the DFT calculations amounts to $d = 2.87(1)$ Å, which is in excellent agreement with the interlayer distance we find in STEM measurements $d = 2.88(3)$ Å. For this structure, the calculations show metallic bands and a high density of states in the Te/Si(111)-(1 × 1) layer at the Fermi energy as shown in Fig. 3. The resulting high carrier concentration potentially results in a high conductivity of the Te/Si(111)-(1 × 1) layer. For the Si(111) bulk, the calculations show a band gap of

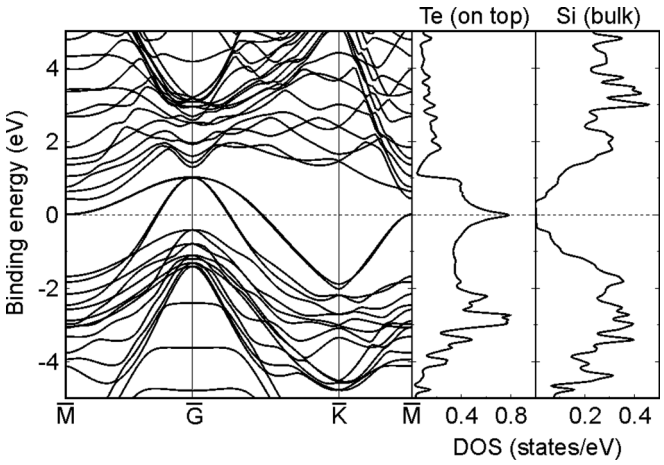


FIG. 3. Calculated band structure and resulting density of states of the Te/Si(111)-(1 × 1) surface in comparison to the Si bulk. The Te layer shows a significant peak in the density of states at the Fermi energy in contrast to the Si bulk, which has a band gap centered at the Fermi energy.

∼1 eV corresponding to the expected literature value. As a result, the Te/Si(111)-(1 × 1) system should be dominated by a two-dimensional conduction channel at the sample surface.

To analyze the conductivity of the Te/Si(111)-(1 × 1) surface experimentally, we use here the approach of *in situ* electrical transport measurements by means of a four-tip STM as the atomically thin Te layer would be irretrievably contaminated and altered when exposed to ambient conditions.

The lateral electrical conductivity of the Te/Si(111)-(1 × 1) surface is hereby measured by contacting the sample with the individual tips of the STM in a four-probe geometry, as described elsewhere [14,25]. This approach allows distance-dependent four-probe measurements of the freshly prepared Te/Si(111)-(1 × 1) surface with the result of the measurement shown in Fig. 4. We find that the distance-dependent four-probe resistance can be described by the analytic solution for a two-dimensional conductor. In Fig. 4 we have also indicated the expected behavior for the bulk with the given bulk resistivity of $\rho_{\mathrm{bulk}} = 22\,\mathrm{k\Omega\,cm}$.

In detail, for equidistant tip spacing a two-dimensional surface conductivity would result in a constant four-probe resistance when varying the tip spacing. However, in the present case we leave three of the four tips at equidistant spacing and move only one tip. The corresponding formulas for the two- and three-dimensional resistivity in this case are [13,14,26]

$$R_{2\mathrm{D}}(x) = \frac{1}{2\pi\sigma_{2\mathrm{D}}}\left[\ln\left(\frac{2s}{x}\right) - \ln\left(\frac{s}{x+s}\right)\right], \qquad (1)$$

$$R_{3\mathrm{D}}(x) = \frac{1}{2\pi\sigma_{\mathrm{bulk}}}\left(\frac{1}{x} + \frac{1}{2s} - \frac{1}{x+s}\right), \qquad (2)$$

with $x$ and $s$ as defined in the inset of Fig. 4. As evident from the formulas, the $x$ dependence of the resulting graph for a three-dimensional bulk dominated sample is distinctly different from the two-dimensional case. Furthermore, for the present sample the expected conductivity arising from the bulk

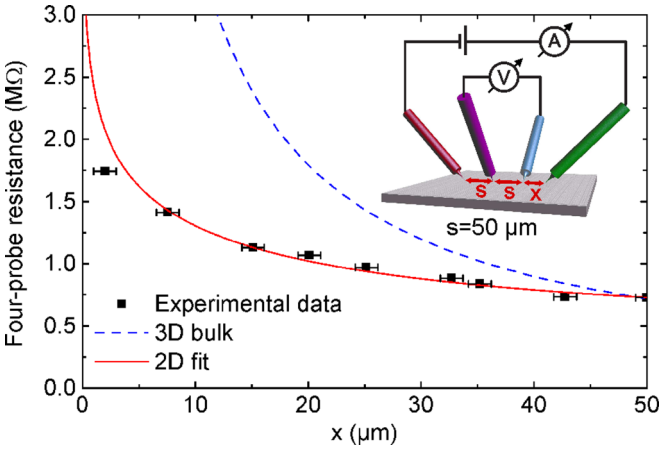


FIG. 4. Distance-dependent four-probe measurement results of Te/Si(111)-(1 × 1) and fit of the corresponding two-dimensional analytical solution (solid red line). The distance-dependent four-probe resistance expected from the pure low doped bulk ($\rho_{\text{bulk}} = 22\,\text{k}\Omega\text{cm}$) is indicated as a dashed blue line. Inset: Schematic of the measurement setup. $s = 50\ \mu$m is kept constant in the measurement while $x$ is varied.

is much lower than the sample conductivity we measure in the experiments. Hereby, the expected bulk conductivity can be reproduced by measurements of the HF treated Si(111) sample surface, before the deposition of Te [14]. We conclude that the bulk conductivity does not play a role in the present measurements. The corresponding Te/Si(111)-(1 × 1) sheet conductivity resulting from fitting Eq. (1) to our experimental data is $\sigma_{2D}^{\text{Te}} = 2.6(5) \times 10^{-7}$ S/□. This value for the Te/Si(111)-(1 × 1) conductivity is relatively small compared to, e.g., $\sigma_{2D}^{\text{Si}} = 5.1(7) \times 10^{-6}$ S/□ of the Si(111)-(7 × 7) reconstruction [14]. This means that, in comparison to a typically even higher TSS conductivity of $\sigma_{2D}^{\text{TSS}} \approx (4-8) \times 10^{-4}$ S/□ [27,28] the Te/Si(111)-(1 × 1) interface contributes only less than 1% of the total conductivity of such a sample. This low observed conductivity at first sight contradicts the large density of states predicted from our DFT calculations. However, we find in the calculated band structure that the largest part of the density of states at the Fermi energy stems from flat bands near the $\overline{\text{M}}$ point which are expected to not contribute much to the electrical conductivity due to their low Fermi velocity [29]. On the other hand, the DFT calculations predict further metallic bands, the unexpected low conductivity of which can be explained by the relatively large surface roughness which we find experimentally. In order to validate the surface structure, we have further tested if the Te/Si(111)-(1 × 1) termination is completely developed by preparation of a sample at a temperature of 350 °C (instead of 270 °C before), where we found no significant variation of the Te/Si(111)-(1 × 1) conductivity compared to the previous measurement. From this finding we conclude that the surface reconstruction is fully developed and stable because otherwise the Te coverage and therefore surface conductivity of the sample would change due to the different equilibrium conditions during the growth.

In conclusion, we report by STEM, STM, LEED, and theoretical calculations that the saturation of an unreconstructed Si(111) substrate surface with Te results in a stable Te/Si(111)-(1 × 1) surface reconstruction. We find experimentally a relatively low electrical conductivity of the sole Te/Si(111)-(1 × 1) surface reconstruction in contrast to a high density of states at the Fermi energy predicted from our DFT calculations. This finding can be partially explained by the low Fermi velocity of the band which contributes the most to the density of states at the Fermi energy. Furthermore, we expect the relatively high surface roughness of the sample surface, due to the initial HF cleaning, to decrease the conductivity with respect to an atomically perfect Te/Si(111)-(1 × 1) layer. However, we would like to stress here that the present preparation procedure is identical to the one used prior to the actual TI film growth and we find the resulting TI films to be of excellent crystalline quality with a sharp interface to the substrate.

Besides the treatment with Te, the saturation of Si(111) substrates prior to vdW epitaxy by, e.g., Se and Bi has also been reported [27,30] and we find the conductivity of the corresponding surface terminations to be not well documented in literature. In general, such interface conduction has to be taken carefully into account not only for topological insulators such as $Bi_2Te_3$, $Sb_2Te_3$, and $Bi_2Se_3$ and corresponding ternary or quaternary materials but also for other vdW materials including GaSe, GaTe, $MoS_2$, $WS_2$, $MoSe_2$, $WSe_2$, and $MoTe_2$.


[1] D. Hsieh, Y. Xia, D. Qian, L. Wray, F. Meier, J. H. Dil, J. Osterwalder, L. Patthey, A. V. Fedorov, H. Lin, A. Bansil, D. Grauer, Y. S. Hor, R. J. Cava, and M. Z. Hasan, Phys. Rev. Lett. **103**, 146401 (2009).

[2] B. Radisavljevic, A. Radenovic, J. Brivio, V. Giacometti, and A. Kis, Nat. Nano **6**, 147 (2011).

[3] K. F. Mak, C. Lee, J. Hone, J. Shan, and T. F. Heinz, Phys. Rev. Lett. **105**, 136805 (2010).

[4] P. Roushan, J. Seo, C. V. Parker, Y. S. Hor, D. Hsieh, D. Qian, A. Richardella, M. Z. Hasan, R. J. Cava, and A. Yazdani, Nature (London) **460**, 1106 (2009).

[5] H. Zhang, C.-X. Liu, X.-L. Qi, X. Dai, Z. Fang, and S.-C. Zhang, Nat. Phys. **5**, 438 (2009).

[6] L. Barreto, L. Khnemund, F. Edler, C. Tegenkamp, J. Mi, M. Bremholm, B. B. Iversen, C. Frydendahl, M. Bianchi, and P. Hofmann, Nano Lett. **14**, 3755 (2014).

[7] Z. Ren, A. A. Taskin, S. Sasaki, K. Segawa, and Y. Ando, Phys. Rev. B **82**, 241306 (2010).

[8] M. Lanius, J. Kampmeier, S. Kölling, G. Mussler, P. Koenraad, and D. Grützmacher, J. Cryst. Growth **453**, 158 (2016).

[9] M. Eschbach *et al.*, Nat. Commun. **6**, 8816 (2015).

[10] A. Koma, Thin Solid Films **216**, 72 (1992).

[11] S. Borisova, J. Krumrain, M. Luysberg, G. Mussler, and D. Grützmacher, Crystal Growth and Design **12**, 6098 (2012).

[12] F. Lüpke, S. Korte, V. Cherepanov, and B. Voigtländer, Rev. Sci. Instrum. **86**, 123701 (2015).

[13] S. Just, H. Soltner, S. Korte, V. Cherepanov, and B. Voigtländer, Phys. Rev. B **95**, 075310 (2017).

[14] S. Just, M. Blab, S. Korte, V. Cherepanov, H. Soltner, and B. Voigtländer, Phys. Rev. Lett. **115**, 066801 (2015).

[15] J. Homoth *et al.*, Nano Lett. **9**, 1588 (2009).

[16] T. Tanikawa, I. Matsuda, T. Kanagawa, and S. Hasegawa, Phys. Rev. Lett. **93**, 016801 (2004).
[17] M. Eschbach *et al.*, Nat. Commun. **8**, 14976 (2017).
[18] Note: The actual sample temperature might be larger by as much as ∼30 K due to operation of the used pyrometer close to its lower-temperature limit.
[19] G. J. Pietsch, U. Köhler, and M. Henzler, J. Appl. Phys. **73**, 4797 (1993).
[20] R. Houbertz, U. Memmert, and R. J. Behm, J. Vac. Sci. Technol. B **12**, 3145 (1994).
[21] G. S. Higashi, R. S. Becker, Y. J. Chabal, and A. J. Becker, Appl. Phys. Lett. **58**, 1656 (1991).
[22] J. P. Perdew and A. Zunger, Phys. Rev. B **23**, 5048 (1981).
[23] E. Wimmer, H. Krakauer, M. Weinert, and A. J. Freeman, Phys. Rev. B **24**, 864 (1981).
[24] For a program description see http://www.flapw.de.
[25] V. Cherepanov, E. Zubkov, H. Junker, S. Korte, M. Blab, P. Coenen, and B. Voigtländer, Rev. Sci. Instr. **83**, 033707 (2012).
[26] P. Hofmann and J. W. Wells, J. Phys.: Condens. Matter **21**, 013003 (2009).
[27] S. Bauer and C. A. Bobisch, Nat. Commun. **7**, 11381 (2016).
[28] F. Lüpke *et al.*, Nat. Commun. **8**, 15704 (2017).
[29] M. D'angelo, K. Takase, N. Miyata, T. Hirahara, S. Hasegawa, A. Nishide, M. Ogawa, and I. Matsuda, Phys. Rev. B **79**, 035318 (2009).
[30] N. Bansal *et al.*, Thin Solid Films **520**, 224 (2011).